Zhou et al. *Microsystems & Nanoengineering* (2026)12:212
https://doi.org/10.1038/s41378-026-01340-y

Microsystems & Nanoengineering
www.nature.com/micronano

ARTICLE Open Access

A smartphone-powered decentralized microfluidic platform for sensitive CRISPR-based nucleic acid detection

Peng Zhou[1], Amber N. McElroy[1], Yingming Xu[1], Andrew Decker[1], Timothy W. Schacker[1], Terrence W. Simon[1], Mark J. Osborn[1]✉ and Tianhong Cui[1]✉

Abstract

Sensitive, portable, and low-cost nucleic acid detection without need for complicated equipment or trained operators, allows flexibility in forward (i.e., near the point of collection) detection and diagnostics that could be applied in resource-limited settings. To this end, we developed a microfluidic, chip-based laser-induced graphene (LIG) heater with precise temperature control for loop-mediated isothermal amplification (LAMP) of DNA or RNA and subsequent CRISPR/Cas9-based molecular interrogation. Detection was pursued using commercial lateral flow assays (LFAs) and an ultrasensitive electrochemical module that utilizes Hexaammineruthenium (III) chloride (RuHex) as a redox probe. Using LIG-based LAMP amplification we were able to amplify and detect targets in samples with as low as 5 copies per 10 µL. We also evaluated post amplification products to determine the threshold amount of analyte required to enable detection. Our device demonstrated detection limits of 10^{11} for LFA and 5×10^6 copies μL^{-1} for the electrochemical platform. An integrated Arduino-based control unit was developed for housing the amplification and detection components of the diagnostic suite, such that it operates solely on smartphone power with steady-state power consumption of approximately 130 mW for the LIG heater. The approach represents a low-cost, low-power diagnostic platform with potential for point-of-care application.

There is a continuous need for smaller and more portable ultrasensitive nucleic acid detection devices for a multitude of uses. It is reported that 47% of the global population lacks access to basic diagnostic services, and this represents a diagnostic gap that negatively impacts the continuum of care. Narrowing this gap to 10% could prevent approximately 1.1 million premature deaths each year with a particularly large impact in rural areas and low-to-middle-income countries[1]. Among existing diagnostic approaches, nucleic-acid testing for identifying RNA and DNA with high specificity and sensitivity would provide a powerful diagnostic platform. However, conventional methods such as reverse transcription quantitative or Polymerase Chain Reaction (RT-qPCR/PCR) largely depend on centralized laboratories, expensive instruments, and trained personnel, leading to extended test-to-result turnaround times that constrain accessibility and limit application in resource-limited settings[2]. Such limitations manifested in the early COVID-19 pandemic, where RT-qPCR test turnaround times often exceeded 24 h, delaying isolation and treatment[3]. This prompted advances in point-of-care diagnostics for detecting peptides/antigens[4]. Nucleic acid–based diagnostic platforms leverage the capabilities of PCR, and instruments such as Abbott's ID NOW (introduced in 2014) and the Cepheid GeneXpert (introduced in 2005) were subsequently adapted for SARS-CoV-2 assays during the COVID-19 pandemic, delivering molecular diagnoses within 5–30 min[5]. Cue Health, Visby Medical, and Lucira further improved portability and

Correspondence: Mark J. Osborn (osbor026@umn.edu) or Tianhong Cui (cuixx006@umn.edu)
[1]University of Minnesota, Minneapolis, MN, USA
These authors contributed equally: Peng Zhou, Amber N. McElroy, Mark J. Osborn, Tianhong Cui.

© The Author(s) 2026
Open Access This article is licensed under a Creative Commons Attribution-NonCommercial-NoDerivatives 4.0 International License, which permits any non-commercial use, sharing, distribution and reproduction in any medium or format, as long as you give appropriate credit to the original author(s) and the source, provide a link to the Creative Commons licence, and indicate if you modified the licensed material. You do not have permission under this licence to share adapted material derived from this article or parts of it. The images or other third party material in this article are included in the article's Creative Commons licence, unless indicated otherwise in a credit line to the material. If material is not included in the article's Creative Commons licence and your intended use is not permitted by statutory regulation or exceeds the permitted use, you will need to obtain permission directly from the copyright holder. To view a copy of this licence, visit http://creativecommons.org/licenses/by-nc-nd/4.0/.

accuracy through disposable, fully-enclosed cartridges[6]. Beyond commercial products, paper-based microfluidic platforms, as demonstrated by Martinez et al., enabled equipment-free nucleic acid amplification and colorimetric detection for pathogen identification[7,8]. Further, fully integrated lab-on-a-chip systems, exemplified by Sun et al., achieved true "sample-to-answer" diagnostics by combining on-chip sample preparation, nucleic acid amplification, and electrochemical detection[9,10].

Among these approaches and systems, the nucleic-acid amplification module is a key consideration for both sensitivity of detection and analytical reliability. Detection of low-abundance targets requires sufficient amplification efficiency to generate a threshold number of molecules for signal detection and measurement[11]. Loop-mediated isothermal amplification (LAMP), with its high specificity and rapid kinetics, has shown to be a powerful method for nucleic acid amplification and molecular diagnostics[12]. However, maintaining precise temperature control for optimal enzymatic activity (60–65 °C) remains challenging, as conventional heaters such as metallic films, resistive wires, and Peltier elements often require high power consumption with its associated elevation in cost[13]. As such, achieving isothermal reaction capabilities under low-power, low-cost conditions remains a major bottleneck in point-of-care performance. Recently, laser-induced graphene (LIG) has emerged as a heating material owing to its excellent electrical conductivity, thermal stability, patternability, and extremely low fabrication cost[14,15]. LIG can be directly patterned on polymer substrates to form flexible heating structures with small dimensions capable of rapid and precise temperature regulation under low voltage while fully meeting the optimal thermal requirements for LAMP reactions[16]. The low-power demand and scalable fabrication make LIG a practical and cost-effective heating solution that is pursued for nucleic acid amplification and detection in the approach presented herein.

Amplification and specific target recognition of nucleic acids are essential for ensuring analytical and diagnostic accuracy. Conventional approaches, such as fluorescent probe hybridization, immunocapture, and enzyme-linked reactions have been widely employed in laboratory diagnostics, yet they typically rely on complex labeling and sophisticated instrumentation[17–20]. The CRISPR-Cas system has emerged as a powerful molecular tool owing to its programmable sequence interrogation capability and its specificity[21]. CRISPR-associated enzymes such as Cas9, Cas12, Cas13 and Cas14, have been explored for nucleic acid diagnostics. Cas12, 13, and 14, upon detection of a target sequence, display indiscriminate trans-cleavage properties that have been harnessed for signal generation using accompanying, collateral reporter nucleic acids[22–26]. Cas9 from *Streptococcus pyogenes* forms a complex with a single-stranded RNA (sgRNA), enabling programmable DNA target interrogation and direct binding with high selectivity and specificity, avoiding the need for optimization of collateral target reporter molecules[27,28]. Cas9 contains two nuclease domains. We and others have shown that the 'dead' Cas9, in which the nuclease domains are inactivated, can be used for diagnostic purposes[29,30].

Point-of-care diagnostic technologies have rapidly advanced through miniaturization of sensing, amplification, and detection systems that enable decentralized healthcare in clinical and resource-limited settings[31,32]. Despite this progress, it remains difficult to achieve a compact platform that integrates low-power amplification, sequence-specific molecular interrogation, and both rapid qualitative and sensitive quantitative readout[33]. Lateral flow assays (LFA) provide rapid, qualitative readouts suitable for on-site screening[34]. However, a threshold number of molecules must be present to enable detection and a readout is dependent on the visual acuity of the operator, which can lead to non-uniformity of evaluation[35,36]. In contrast, electrochemical signals enable highly sensitive, unambiguous, and quantitative analysis[37–39]. To further realize the promise of Cas9-based diagnostics, the present study pursued comparative analyses between LFAs and a new design of an electrochemical module. The result of these efforts is an integrated nucleic-acid detection system that enables both qualitative and quantitative analyses within a single, portable platform. The system to be presented incorporates a LIG heater that enables on-chip LAMP for efficient nucleic acid amplification. Products can be analyzed through two complementary pathways using CRISPR/Cas9: an LFA for rapid qualitative screening, and an electrochemical detection module for highly sensitive and quantitative analysis. The amplification and detection components were compactly integrated within a microfluidic architecture and the entire system operates via smartphone-based power and control, offering portability and low energy consumption for field deployability.

Results and discussion

Principle and system design of an integrated sensing platform

The overall rationale, architecture, and design concepts of the present nucleic acid detection system are illustrated in Fig. 1. Centralized laboratory-based diagnostics rely on complex instrumentation and require trained personnel that contribute to longer turnaround times and limited accessibility and applicability. Diagnostic workflows consist of several sequential steps, including sample collection, lysis, nucleic acid extraction, amplification, and detection. Herein, the focus is on LAMP-based nucleic acid amplification and CRISPR/Cas9-mediated target

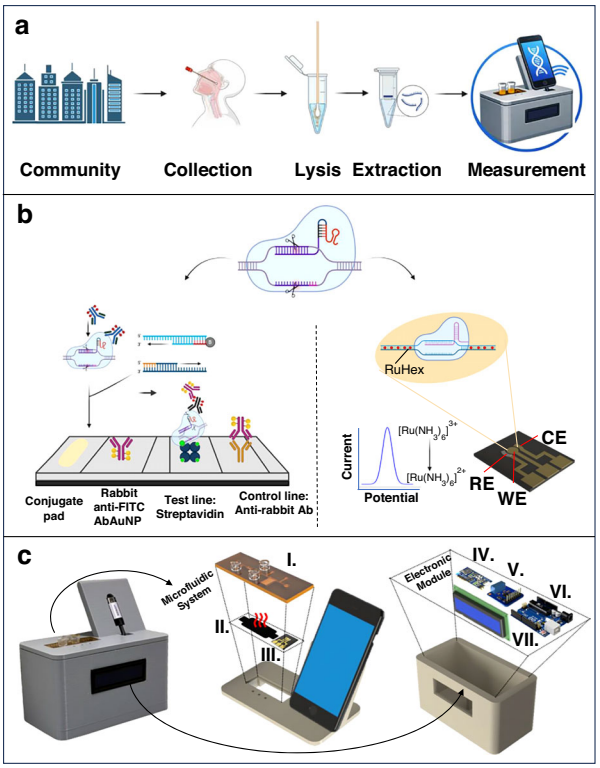


Fig. 1 Schematic of testing workflow and system architecture. **a** Schematic illustration of the testing workflow. **b** Schematic illustration of the Cas9-based detection modules, including both lateral flow assay (left) and electrochemical (right) sensing strategies. WE working electrode, RE reference electrode; CE counter electrode. **c** Integrated system architecture. Microfluidic system (I) microfluidic chip, (II) LIG heating module, (III) electrochemical sensor; electronic module: (IV) miniaturized potentiostat, (V) MAX31856 thermocouple amplifier, (VI) Arduino control unit, and (VII) display

interrogation. In the present system, Cas9 serves as the central molecular recognition element, enabling dual-mode nucleic acid detection via either LFA or electrochemical analysis. LAMP amplification and electrochemical detection modules are integrated into a single device, simplifying the workflow and promoting portability of the diagnostic platform (Fig. 1a).

Programmable DNA binding is facilitated by an sgRNA, a small transcript with 20 nucleotides of homology to a target sequence and a scaffold that leads to complexation with *Streptococcus pyogenes* Cas9 nuclease (Fig. 1b)[40]. For visual detection, commercial LFAs are employed that require the analyte to be conjugated/bound by biotin and fluorescein isothiocyanate (FITC). To accomplish this for nucleic acids, LAMP primers were developed for a region of the Spike (S) gene of SARS-CoV-2 (Supplementary Fig. S1A). A biotinylated LAMP primer set was evaluated and identified (Supplementary Fig. S1B) for incubation with Cas9:SARS-CoV-2 sgRNA and an anti-Cas9 FITC-labeled antibody to fulfill the labeling requirements for LFA detection (Supplementary Fig. S1C). Upon sample addition, the target analyte is labeled on the conjugation pad by gold nanoparticles conjugated to anti-FITC antibodies, and the resulting complexes accumulate at the test line containing streptavidin. (Fig. 1b).

Cas9 was further employed to achieve a high-sensitivity quantitative analysis with an electrochemical sensing module. A Cas9:sgRNA complex was immobilized on an electrode surface as a molecular recognition unit. RuHex served as a redox-active probe, electrostatically interacting with the phosphate backbone of target DNA captured by interaction with Cas9. Variations in probe binding were evaluated by monitoring electrical current changes using Differential Pulse Voltammetry (DPV), allowing molecular recognition events between Cas9 and a specific nucleic acid target to be quantitatively converted into electrical signals.

The complete platform consists of an electronic control module and a microfluidic subsystem (Fig. 1c). To integrate and house these components, the electronic module was designed to include a miniaturized potentiostat capable of network-based communication with a smartphone, a MAX31856 thermocouple amplifier for temperature monitoring, an Arduino-based control unit, and a compact display interface. The microfluidic subsystem integrates a LIG heater, an electrochemical sensor, and a microfluidic chip. The entire system operates solely on smartphone power, requiring no external device or power supply. A custom-designed 3D-printed enclosure offered structural stability and a small footprint while also minimizing manufacturing cost.

Design and optimization of an on-chip LAMP module

To achieve stable and uniform heating for on-chip amplification using LAMP, a LIG film was employed as the heating element. The LIG was fabricated via CO_2 laser scribing of a polyimide substrate, resulting in a porous, conductive carbon network possessing favorable thermal and electrical properties. The porous morphology, as shown in the scanning electron microscopy (SEM) images (Fig. 2a, b), facilitates rapid heat distribution and uniform temperature control across the microchip. Raman spectroscopy of the LIG film (Fig. 2c) shows the characteristic D (~1350 cm^{-1}) and G (~1580 cm^{-1}) Raman bands. They are established signatures of graphitic carbon with partial disorder that supports its high electrical conductivity and mechanical robustness and underscores suitability for heater applications in compact analytical devices[41].

Temperature regulation was achieved through an Arduino-based feedback control system. An Arduino Uno R3 monitored the thermocouple output and maintained temperature stability using the proportional–integral–derivative (PID) control algorithm[42]. The error between the measured and set-point

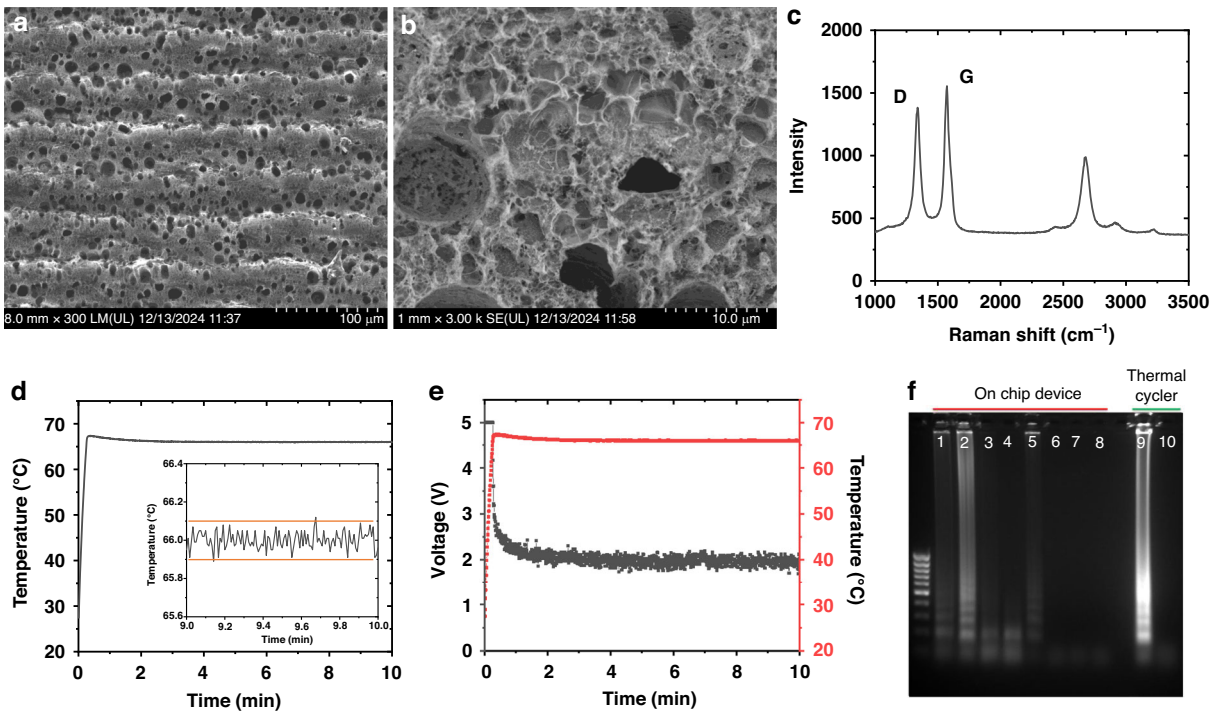


Fig. 2 Structural and performance characterization of the on-chip LAMP module. SEM images of the LIG heater at low **a** and high **b** magnification. **c** Raman spectrum of the LIG heater. **d** Temperature control profile showing heating within 10 min; inset: zoomed-in view of stable temperature regulation. **e** Correlation between heating voltage and temperature. **f** Gel electrophoresis of on-chip LAMP amplification using SARS-CoV-2 DNA. Lanes 1–4: 65–68 °C on-chip device with target DNA; Lanes 5–8: 65–68 °C on-chip device without target DNA; Lanes 9–10: commercial thermal cycler (65 °C) with/without target DNA

temperatures serves as the feedback signal. The output of the PID loop determines the power supplied to the heater via a pulse-width modulation signal at 980 Hz. When the measured temperature varies from the set point, the system automatically increases or decreases heater power. As a result, the sample temperature is stabilized and maintained within a narrow ±0.1 °C range, as demonstrated in the heating profile shown in Fig. 2d. The relationship between heater voltage and temperature is illustrated in Fig. 2e: the device is initially powered at 5 V to accelerate heating from room temperature to 66 °C, and then stabilized at an average operating voltage of approximately 1.98 V. Considering a heater resistance of 30 Ω, the steady-state power consumption is approximately 130 mW, accomplishing low energy demand and making it suitable for sources of minimal power such as a smartphone.

With this design, on-chip LAMP amplification temperatures were assessed and optimized for efficient nucleic-acid amplification. Considering the potential temperature gradient between the LIG heater surface and the reaction solution, experiments were performed at four set-point temperatures ranging from 65 °C to 68 °C using SARS-CoV-2 target DNA as a nucleic acid template for LAMP. Agarose gel electrophoresis was employed to assess amplification and the results (Fig. 2f) show amplification at 65 °C and 66 °C (lanes 1–2), with greater efficiencies observed at 66 °C. When the temperature was further increased to 67 °C and 68 °C (lanes 3–4), amplification products were still detectable but with substantially reduced efficiency compared with 66 °C, indicating decreased polymerase activity at elevated temperatures. Control experiments without target DNA were conducted under the same temperature conditions (lanes 5–8). The observated optimal on-chip LAMP temperature was 66 °C, which is slightly higher than the standard 65 °C recommended by the manufacturer for LAMP. This small deviation can be attributed to the difference between the measured LIG surface temperature and the actual solution temperature, as the thermocouple senses the heater, rather than the liquid. To further validate system reliability, the on-chip LAMP results were compared with those obtained using a commercial thermal cycler set at 65 °C. Consistent outcomes were observed for both the target-containing lane (lane 9) and the negative control lane (lane 10) samples, confirming that the on-chip platform achieves high amplification efficiency compared to that of a benchtop thermocycler/heat block instrument.

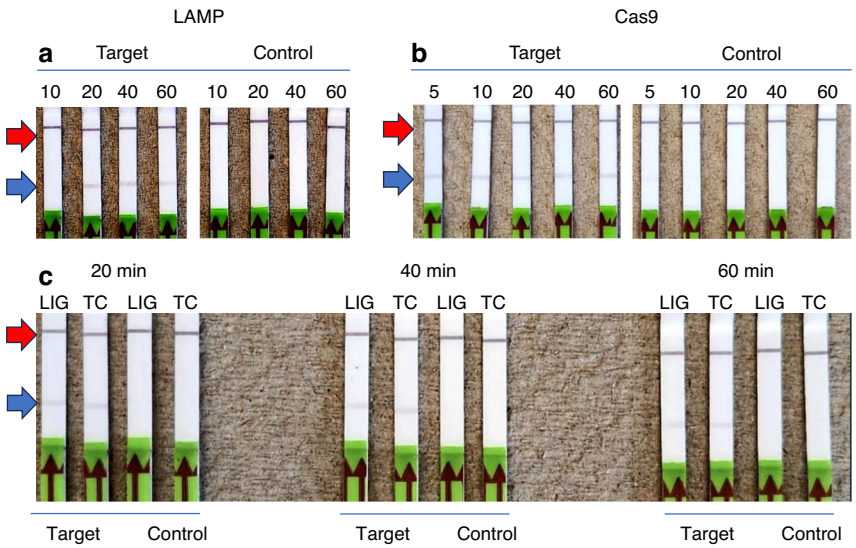


Fig. 3 Amplification and detection optimization and LIG comparison to the thermocycler. a LAMP of SARS-CoV-2 RNA (10 total copies of template in a 20 µL solution) under different durations of 60 °C incubation for LAMP (indicated above the LFA strips in minutes) followed by LFA analysis. **b** Incubation of biotinylated LAMP products at 37 °C with Cas9:sgRNA:FITC antibody complexes for the indicated reaction times (in minutes above the LFA strips). **c** LIG and thermocycler LAMP comparison. Ten copies of SARS-CoV-2 were used as templates for LIG or thermocycler (TC) LAMP amplification of 30 min each. Products were then tested at different incubation times with Cas9:sgRNA (timepoints shown above LFA). Target and control strip labeling is shown below, the control is a non-homologous sgRNA. The blue arrow is the test band, and the red arrow is the control band for the LFA analysis

CRISPR–Cas9-based LFA for visual nucleic acid detection

Previously, a biotinylated, 'dead' Cas9 was employed for LFA under reaction conditions exceeding 2 h[30]. This version of the Cas9 enzyme did not possess nuclease activity and was lyophilized, requiring resuspension and lengthy reaction conditions prompting the pursuit of identification of optimized detection conditions. As such, off-the-shelf reagents were employed, including high concentration (10 mg/mL) recombinant Cas9 nuclease supplied in a glycerol buffer that did not require resuspension, an anti-Cas9 FITC antibody, and a biotinylated primer for PCR/LAMP amplification. These ready-to-use reagents worked in concert to allow analyte labeling with FITC and biotin for detection of biotinylated nucleic acids using commercial LFA strips. We varied the LAMP or Cas9 incubation periods and performed comparisons using the LIG heater and a laboratory thermocycler. With a thermocycler, we observed that 20-min reaction/incubation for both LAMP and Cas9 enabled detection by LFA (Fig. 3a, b). Interestingly, prolonged Cas9 incubation appeared to diminish the LFA test band intensity. We hypothesize that this may be due to the employment of Cas9 nuclease and its endonucleolytic cleavage of the biotinylated target amplicon that may uncouple the requisite biotin:FITC conjugate for LFA.

LIG LAMP amplified products were next incubated with Cas9 at 37 °C, either on a LIG or a thermocycler, at multiple times (Fig. 3c). These data demonstrate that LIG with a low power requirement can mediate LAMP amplification for follow-on CRISPR-based LFA detection. Negative controls using non-homologous sgRNA showed no visible test line, confirming high reaction and target specificity.

With a goal of making diagnostics streamlined and portable, and giving a ready-to-use format of Cas9, the anti-Cas9 antibody, and LFAs of long-term storage conditions of the Cas9:sgRNA:anti-Cas9-FITC complex were also evaluated. Cas9 nuclease/FITC antibody complexes were incubated for up to 7 days at room temperature, refrigeration of +4, −20, and −80 °C. Room temperature and refrigeration were suitable for the short term (up to 4 days) while cold storage of 4 °C to −80 °C enabled detection for at least 7 days (Supplementary Fig. S2). These results identified the reaction and storage conditions for LFA-based nucleic acid detection with Cas9.

Detection capability depends on assay sensitivity related to the amount of analyte present in the sample. At extremely low template concentrations, amplification events follow Poisson sampling statistics, meaning that detection from single-copy inputs is inherently probabilistic rather than deterministic. To evaluate amplification sensitivity, PicoGreen analysis was used to quantify targets followed by serial dilutions of the SARS-CoV-2 RNA transcripts to approximate a range of template copy numbers. In these experiments, LAMP amplification with LFA readout was observed from samples estimated to contain a putative

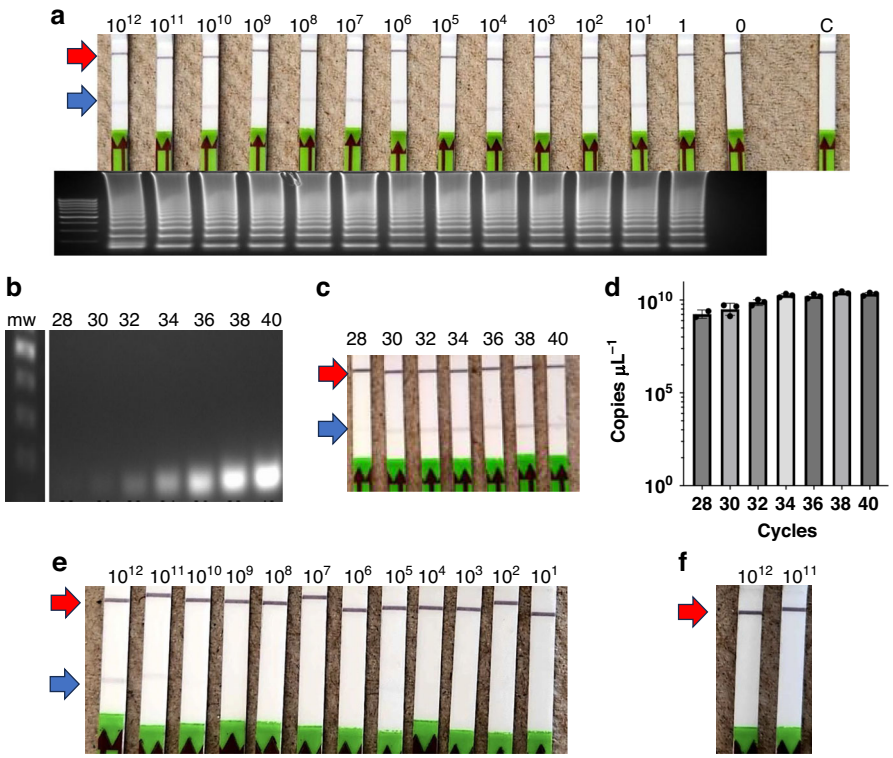


Fig. 4 Assessment of the Cas9-based LFA detection sensitivity limits. a Serially diluted SARS-CoV-2 RNA templates amplified by LAMP and analyzed by LFA (top) and agarose gel electrophoresis (bottom). The label above the LFA strips shows the input amount of starting template. Representative of 3/5 replicates. **b** PCR amplification was performed under standard thermal cycling with reactions terminated at the indicated cycle numbers for analysis by agarose gel. **c** LFAs were performed on the DNA from each cycle number indicated. **d** PCR amplicons underwent quantification and the amount of DNA for samples in triplicate are shown as the mean and SEM in the total 20 microliter of reaction volume. The x-axis is the cycle number. **e** Known copy numbers (shown above the LFA and defined by PicoGreen) of DNA to mimic post amplification yields, were incubated with Cas9:sgRNA:FITC antibody for 60 min and then evaluated by LFA. **f** A control using a mismatched sgRNA and 10^{12} or 10^{11} DNA copies μL^{-1} is shown. In all LFAs, the red arrow is the control line and the blue arrow is the test line

single copy of target RNA (Fig. 4a). These observations are consistent with previous work demonstrating that LAMP can achieve amplification from single-copy nucleic acid inputs under optimized conditions[43].

These data show that low copy number amplification is achievable by LAMP under laboratory conditions; however, template concentration, amplification efficiencies, and total yields may vary from patient to patient and/or sample to sample. To determine whether a threshold number of post amplification molecules must be present, related to the amplification efficiency of a polymerase (i.e., LAMP), two approaches were employed. First, thermocycler-based PCR was performed and halted at various cycles to model conditions where amplification efficiencies may be lacking (e.g., target degradation, PCR inhibitors etc.). A visible LFA signal was observed from target nucleic acid generated by 30 PCR cycles, which correlates with the electrophoretic sensitivity of agarose gel analysis (Fig. 4b, c). In parallel, the amount of amplified DNA yielded at each of these cycles was quantified using PicoGreen[44] (Fig. 4d). Serially diluted DNA was then prepared to evaluate the LFA detection limit related to total amount of DNA that was determined to be approximately 1×10^{11} copies per 20 µL (~5×10^{9} copies μL^{-1}) (Fig. 4e). For each experiment, we employed a mismatched sgRNA that was also tested at high DNA concentrations (10^{12} and 10^{11} copies μL^{-1}). No detectable LFA signal was observed (Fig. 4f).

Specificity is afforded both by Cas9 and LAMP amplification. The LAMP primer set was optimized (Supplementary Fig. S1) as well as Cas9 conditions (Figs. 3, 4, and Supplementary Fig. S2). For additional specificity studies, a biotinylated and competing genomic DNA that bore no homology to the target was generated and interrogated with SARS-CoV-2 sgRNA. Non-homologous, biotinylated DNA did not cross-react with Cas9:SARS-CoV-2 and sgRNA (Supplementary Fig. S3A). A mixture of non-homologous and SARS-CoV-2 DNA still resulted in an LFA band; however, the intensity was somewhat diminished (Supplementary Fig. S3B). We postulate that employment of a 50:50 ratio of target and non-homologous DNA as a result decreases the amount of

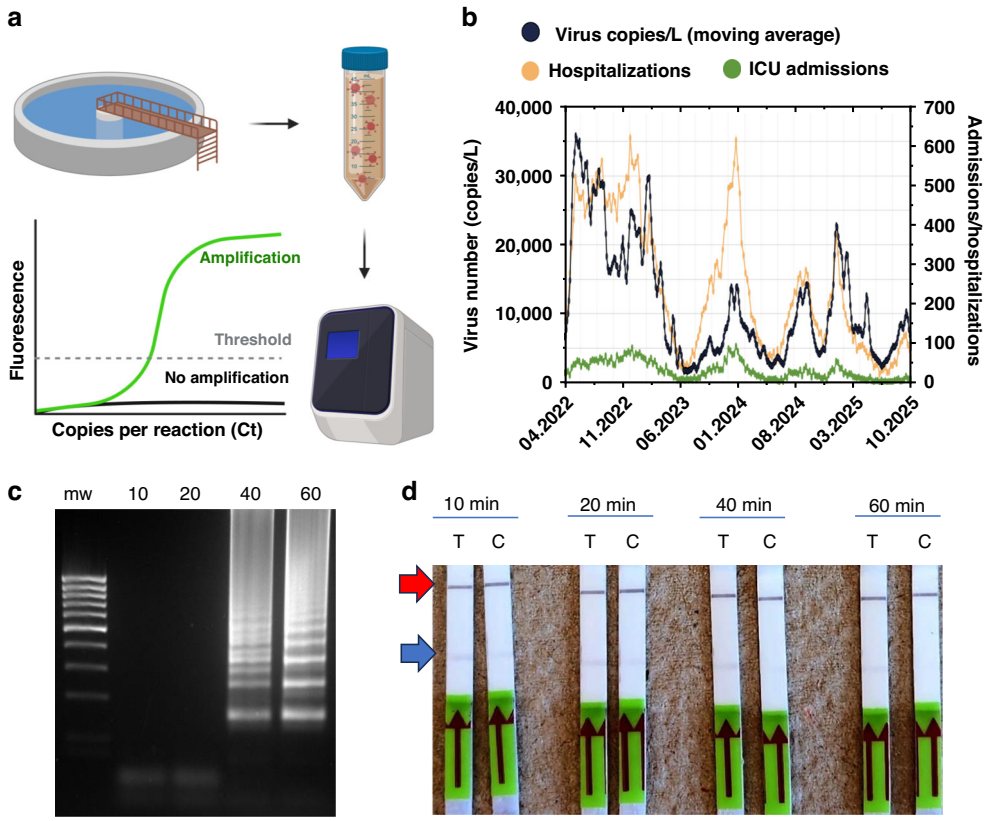


Fig. 5 Cas9-based LFA testing of wastewater samples. a Wastewater pathogen detection program sample analysis. **b** Graph shows quantitative RT PCR data as virus copies per liter of wastewater influent (left y-axis; black line) along with hospital (yellow) and intensive care unit (green) patient admissions (right y-axis) across the state of Minnesota from April 2022 to February 2026 (https://wastewater.uspatial.umn.edu/sars-cov-2/). **c**, **d** Influent wastewater nucleic acid assessment by LFA. (**c**) RT-LAMP was applied for the indicated duration (10, 20, 40, or 60 min) and then resolved on an agarose gel. **d** 60-min RT-LAMP sample was incubated with Cas9:sgRNA:FITC Ab for specified times ranging from 10 to 60 min (time of incubation indicated above LFA) and then examined by LFA. Above the LFA the labeling indicates which samples were incubated with a SARS -CoV-2 sgRNA (T target) or an unrelated sgRNA (C control). Red and blue arrows are the control and test bands, respectively

target amplicon available for detection. Accordingly, a rigorous LAMP PCR primer design framework is developed that would ensure maximum target product amplification efficiencies with minimized off-target amplicon generation.

Under these defined operating principles, real-world samples are evaluated. Since early in the pandemic, a wastewater-based public health laboratory has been operated, containing composite influent samples from sewage treatment sites. The viral load levels of these samples were benchmarked against community-level hospitalizations (Fig. 5a, b), with a turnaround time of 48–72 h from collection to PCR results[45]. The standard operating procedure involves shipment of samples to the laboratory for nucleic acid isolation and qRT-PCR using the TaqPath™ assay that simultaneously, in a multiplex fashion, evaluates the N-, S-, and Orf1a genes of SARS-CoV-2[46]. Wastewater total nucleic acid isolated by column purification underwent LAMP amplification for 10, 20, 40, or 60 min, and agarose gel analysis was performed (Fig. 5c). Following this, using 60-min LAMP incubation for amplification, the duration of Cas9 incubation was evaluated, demonstrating detection of experimental but not control samples at >40 min (Fig. 5d). TaqPath™ qRT-PCR data were presented in Supplementary Fig. S4 that notably shows S gene target failure consistent with the Omicron variant and its two amino acid deletion in the S gene (H69V70)[47]. Importantly, our employed SARS-CoV-2 sgRNA spans H69V70 allowing discrimination of this sequence by Cas9, showing detection of Omicron SARS-CoV-2 by LFA (Fig. 5d).

The results in Figs. 3 and 4 demonstrate LFA-based detection of SARS-CoV-2 in real-world wastewater samples using commercially available reagents. While LFA offers simplicity and high specificity with Cas9, its reliance on threshold analyte levels and visual interpretation may limit sensitivity and diagnostic accuracies[48]. This motivated the development of a LIG-based electrochemical readout to enhance and maximize detection performance.

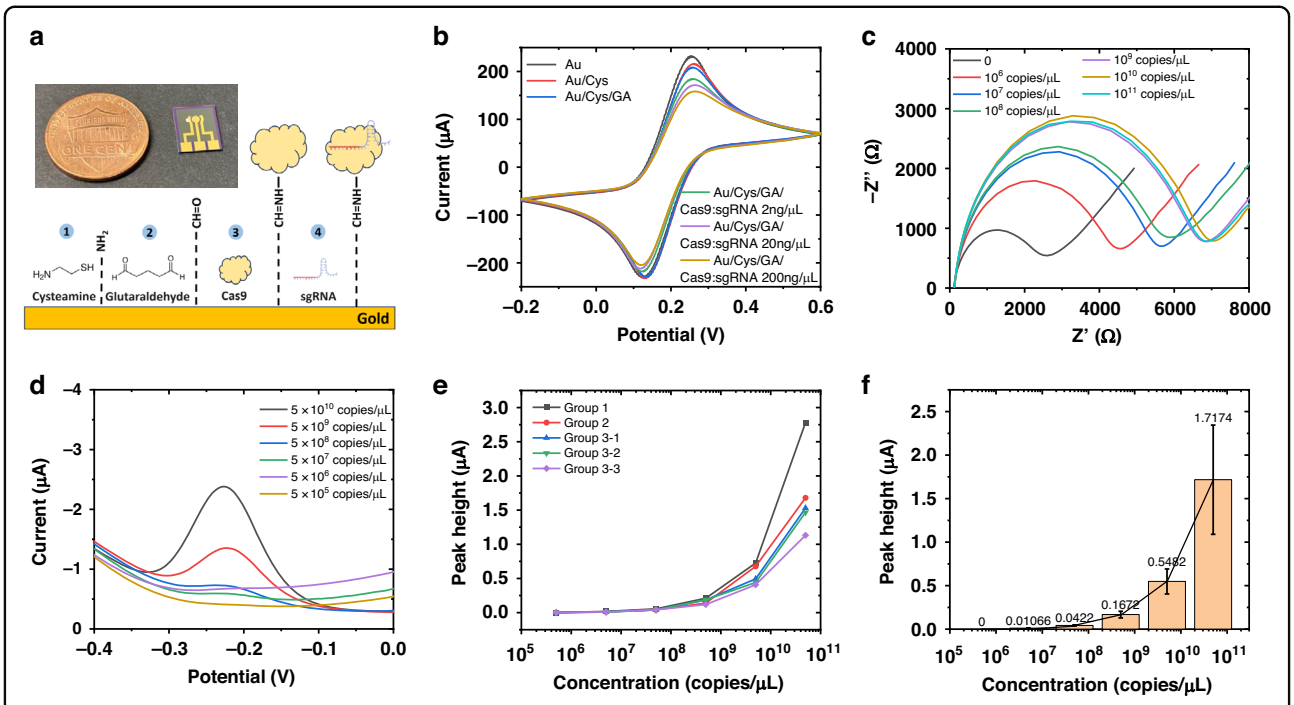


Fig. 6 Characterization of the Cas9-based electrochemical sensing platform. a Schematic diagram of the electrode size and surface modification process. **b** CV curves of the electrode after each modification step and with different Cas9–sgRNA complex concentrations. **c** EIS spectra of electrodes incubated with DNA solutions of varying concentrations. **d** DPV responses of the sensor at different DNA concentrations. **e** Statistical summary of DPV responses from repeated measurements. **f** Calibration plot of peak current versus DNA concentration

Cas9-based electrochemical nucleic acid detection

An electrochemical sensing platform was developed (Fig. 6) to enable nucleic acid detection with quantitative metrics. The sensor employs a standard three-electrode configuration with a gold working electrode. The surface modification process is illustrated in Fig. 6a, where cysteamine (Cys) and glutaraldehyde (GA) are sequentially used as molecular linkers to immobilize the user-designed Cas9–sgRNA complex. The modification steps were characterized by cyclic voltammetry (CV) in a 5 mM ferri/ferrocyanide solution (Fig. 6b). With each modification layer, the redox peak current gradually decreased, indicating the formation of an organic molecular layer on the electrode surface that hindered the charge transfer of electroactive species at the interface. As shown in Fig. 6b, the concentration of the Cas9–sgRNA complex had a significant effect on modification efficiency—higher concentrations led to greater suppression of the redox peak current, suggesting that more Cas9–sgRNA complexes were immobilized on the electrode surface.

Optimization experiments (Supplementary Fig. S5) were pursued using various amounts of Cas9, RuHex and incubation periods. This identified conditions of: Cas9 concentration of 200 ng μL^{-1}, a DNA incubation time of 10 min, a RuHex concentration of 50 μM with an incubation time of 5 min. The binding of target DNA to the immobilized Cas9–sgRNA complex was verified by electrochemical impedance spectroscopy (EIS). Note that RuHex electrostatically binds to the phosphate backbone of DNA and is reduced from $RuHex^{3+}$ to $RuHex^{2+}$ during measurement, producing a reduction peak that is proportional to the amount of bound DNA, (Fig. 6c). The charge-transfer resistance (Rct) increases progressively with DNA concentration and saturates at approximately 10^9 copies μL^{-1}.

For quantitative analysis, DPV was performed after RuHex incubation with known amounts of input target nucleic acid (Fig. 6d). The reduction peak current increases with rising DNA concentration while signals disappear entirely when the concentration is below 5×10^6 copies μL^{-1}. Three groups of DNA samples with identical concentrations were tested to evaluate reproducibility, with one group measured in triplicate (Supplementary Fig. S6). The summarized results in Fig. 6e show a consistent trend of peak current increasing with DNA concentration, demonstrating repeatability across groups. The averaged calibration curve (Fig. 6f) exhibits a logarithmic response, yielding a detection limit of 5×10^6 copies μL^{-1}, which is three orders of magnitude more sensitive than that from the LFA method. Control experiments using high concentrations of non-target DNA amplicons (5×10^6 copies μL^{-1}) produced no detectable redox peak (Supplementary Fig. S6F),

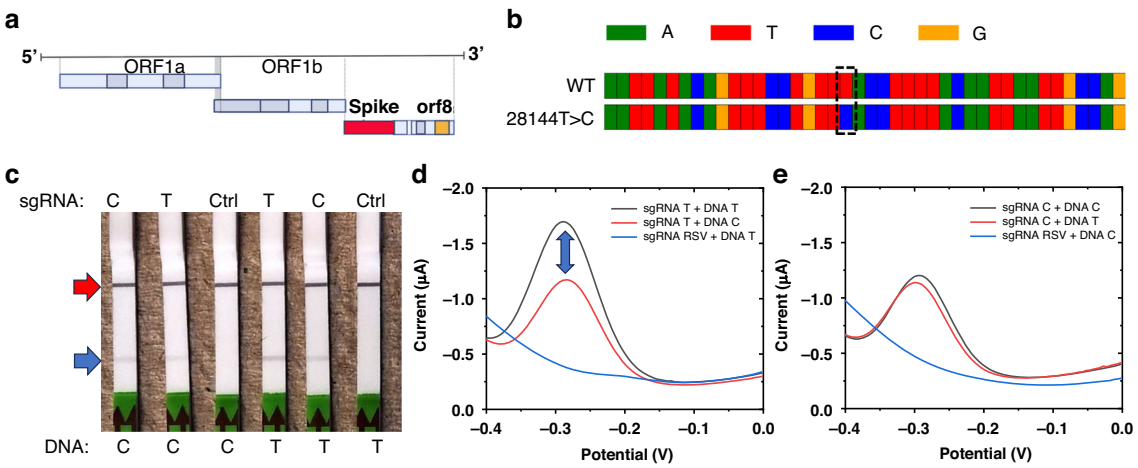


Fig. 7 Evaluation of detection selectivity of the Cas9-based sensing platforms. a Schematic of the SARS-CoV-2 genome highlighting the ORF8 gene region used for selectivity testing. **b** Sequence alignment of wild-type (WT) and mutant targets showing a single-base substitution at position 28144 (T→C). **c** LFA results obtained using sgRNAs targeting either C or T, with corresponding DNA templates. The red and blue arrows indicate control and test lines, respectively. **d** DPV responses of the electrochemical sensor using sgRNA T with DNA T and DNA C templates. **e** DPV response of the sensor using sgRNA C with DNA C and DNA T templates. Controls are SARS- CoV-2 amplicons with an sgRNA for the respiratory syncytial virus (RSV)

confirming that signal generation depends on specific Cas9/sgRNA mediated target recognition.

The CRISPR/Cas9 system can show specificity down to single nucleotide resolution, depending on the sequence complexity and the sgRNA design[49,50]. Previously, this group developed reagents to assess the discriminatory capabilities of Cas9 for a single nucleotide variant, either thymine (T) or cytosine (C), at position 28144 in the ORF8 gene of SARS-CoV-2 that can play a role in immune evasion[51,52]. These previous efforts required high salt concentrations and significant optimization to achieve SNP resolution detection. The capability of the electrochemical method versus LFA was pursued in the present study using a target sequence containing T or C (designated DNA_T or DNA_C) with corresponding sgRNA_T or sgRNA_C (Fig. 7a, b). The results (Fig. 7c–e) showed that both platforms produced stronger signals when the sgRNA was fully matched to the target DNA, whereas single-base mismatches led to significantly attenuated responses. Considering that the electrochemical sensor's output current exhibits an exponential relationship with DNA concentration, the reduced signal intensity shows a substantial decrease in DNA binding under mismatch conditions which confirms the high single-nucleotide selectivity of the Cas9-based sensing system. The electrochemical sensor exhibited superior differentiation capability compared with LFA, as it generated distinguishable signals for both matched and mismatched samples.

Interestingly, the signal intensity obtained from the T–T matched pair was consistently higher than that of the C–C pair. This difference may have originated from intrinsic thermodynamic variations between sequences: thymine-rich regions generally exhibit lower local duplex stability and weaker base stacking interactions, facilitating R-loop formation and enhancing sgRNA–DNA hybridization efficiency[51]. Previous studies had demonstrated that Cas9 binding kinetics and cleavage efficiency are strongly influenced by target GC content and local structural energy; GC-rich regions form more stable duplexes that hinder R-loop propagation, whereas AT-rich regions promote effective Cas9–sgRNA complex formation[53].

System integration and operation

An enclosed microfluidic platform was developed (Fig. 8) for achieving unified integration of nucleic acid amplification and electrochemical detection. The system combines the LIG-based on-chip LAMP heating module with the Cas9-based electrochemical sensing unit, enabling fully enclosed molecular detection from amplification to signal readout. The chip was fabricated from laser-cut polymethyl methacrylate (PMMA) layers bonded with polyimide double-sided adhesive. It consists of two serially-connected chambers: a front heating chamber for LAMP amplification with a backside LIG heater that provides precise temperature control and a rear sensing chamber with an embedded electrochemical sensor for Cas9-mediated DNA capture and signal transduction.

Fluid transfer between chambers is regulated by three manually operated PDMS micro-pumps that sequentially control solution injection, transfer, and reaction steps (Fig. 8a). The infrared thermal image of the LIG heater

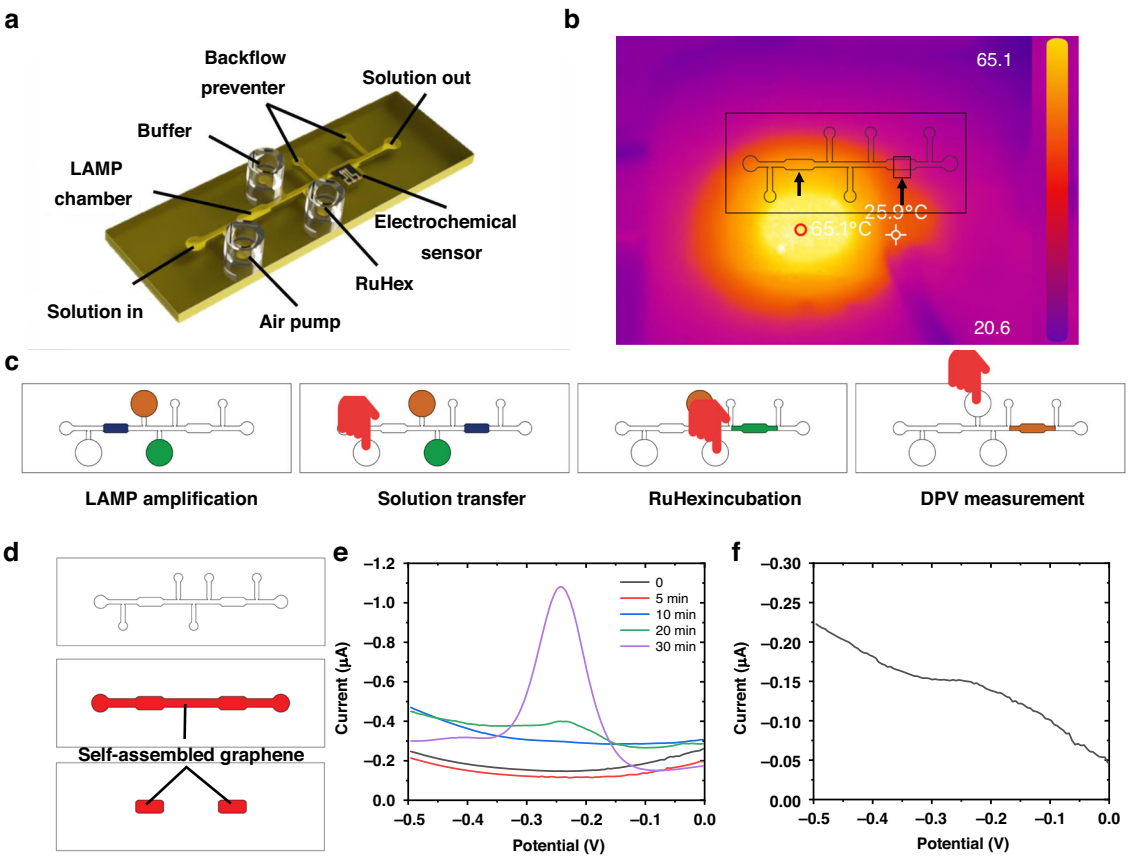


Fig. 8 . Integrated microfluidic system. **a** Schematic of the integrated microfluidic system. **b** Infrared thermal image of the device showing the temperature distribution during operation. **c** Operational workflow of the integrated device. **d** Self-assembled graphene oxide coating on the microchannel surface. **e** DPV responses of the electrochemical sensor with different amplification times. **f** Baseline-subtracted DPV response of the electrochemical sensor after 10 min of amplification

operating at the LAMP amplification temperature is shown in Fig. 8b. A uniform temperature distribution is observed within the amplification chamber while the temperature in the electrochemical detection chamber remains at 25.9 °C, ensuring Cas9 activity preservation without thermal inactivation.

The operational workflow is illustrated in Fig. 8c. The first micro-pump transfers the amplified LAMP solution from the heating chamber to the sensing chamber where target DNA is captured by Cas9–sgRNA complexes immobilized on the electrode surface. The second pump then introduces the RuHex solution, allowing electrostatic binding between RuHex and the captured target DNA. Finally, the third pump delivers the DPV buffer solution to remove unbound RuHex and establishes a stable electrochemical measurement environment. A detailed video demonstration of the complete process is provided in Supplementary Video 1.

To prevent liquid backflow or cross-contamination upon pump release, two open-type backflow preventers were installed between the inlet and outlet, ensuring unidirectional fluid and separation from the waste solution. To enhance internal fluid transport, the microchannels were modified to be hydrophilic, using self-assembled graphene oxide. As shown in Fig. 8d, one side of the channel was fully coated with graphene oxide to improve hydrophilicity, while only the chamber regions on the opposite side were selectively treated to confine liquid flow. Contact angle measurements (Supplementary Fig. S7) indicate that graphene modification reduced the surface contact angle from 70° to 30°, confirming significantly enhanced hydrophilicity and improved flow stability within the microchannel. These segregated flow directions and characteristics, along with the use of LAMP with uracil-DNA-glycosylase and uracil triphosphate for DNA synthesis, serve to mitigate or eliminate cross over and carry over contamination risks[54].

An electronic control module is integrated and all components are housed in a 3D-printed enclosure, ensuring compact assembly and coordinated operation. The electronic system includes an Arduino control unit, a MAX31856 thermocouple amplifier, and a miniaturized potentiostat for unified regulation of temperature,

Table 1 Comparison of representative portable nucleic acid amplification tests platforms

System	Amplification	Sensing	LoD (approx.)	Time-to-result	Power
Abbott ID NOW	Isothermal (NEAR)	Fluorescence	125 copies/mL	15 min	mains-powered
Cepheid GeneXpert	RT-PCR	Fluorescence	500 copies/mL	30 min	mains-powered
Roche cobas Liat	RT-PCR	Fluorescence	100 copies/mL	20 min	mains-powered
Cue Health	Isothermal NAAT	Electrochemical	20 copies/Sample	20 min	Battery-powered
Lucira	RT-LAMP	Colorimetric	1000 copies/mL	30 min	Battery-powered
This work	LAMP	Electrochemical	5 copies/10 μL	30 min	Smartphone-powered

electrochemical measurements and data processing[55]. The display interface provides step-by-step prompts for each manual micro-pump actuation, ensuring precise timing and reproducibility during operation. The overall working process of the integrated system, including heating, liquid transfer, reaction, and detection, is demonstrated in Supplementary Video 2.

To validate the performance of the integrated platform, DNA solutions containing as low as 5 copies per 10 μL were subjected to amplification and then detected. As shown in Fig. 8e, f, a weak electrochemical signal appeared after 10 min of LAMP amplification, became clearly distinguishable at 20 min, and progressed to peak signal intensity after 30 min. These results indicate that the platform can detect as low as 5 copies per 10 μL of DNA with a detection window of 30 min.

Table 1 compares the proposed platform under representative commercialized portable nucleic acid amplification tests (NAATs). In contrast to systems that rely on dedicated instrumentation and external power (e.g., Abbott ID NOW, GeneXpert, and cobas Liat), as well as portable devices requiring integrated readers or built-in power (e.g., Cue Health and Lucira), the approach/platform described herein achieves competitive sensitivity while enabling low-power, quantitative electrochemical detection, enhanced portability and suitability for field-deployable applications.

Conclusion

Previous efforts employing Cas9 as detection platforms for LFA were expanded for employment of off-the-shelf commercial reagents and development of an electrochemical device. Cas9–sgRNA complexes can be stored, making them amenable to develop and archive strategic reserves for pathogens of interest. For LFA detection, a threshold number ($\sim 1 \times 10^{11}$) of copies must be produced during amplification. Despite no cross-reactivity when employing non-homologous sgRNA or DNA amplicons, lower resolution specificity was prevalent when SNP detection and discrimination was undertaken. This could lead to false positives for selected high homology targets and could require interpretation of LFAs in a non-standard format (individual operation visualization), prompting pursuit of more streamlined and sensitive methods.

Thus, we sought to merge amplification and detection into a modular device for improvement of sensitivity and specificity. A fully integrated microfluidic platform combining LAMP amplification, CRISPR/Cas9 molecular recognition, and dual-mode detection with low power requirements for portable and quantitative nucleic acid analysis was developed. A graphene heater fabricated using laser-writing provided rapid and stable temperature control, enabling precise on-chip isothermal LAMP amplification. This LIG supported readouts by either LFA or an electrochemical biosensor. The latter offered a significantly enhanced overall analytical sensitivity with a limit of 5×10^6 copies μL^{-1}, representing three-orders-of-magnitude improvement in sensitivity compared with LFA. When combined with a 10-min LAMP amplification step, the electrochemical biosensor enabled reliable detection of as low as 5 copies per 10 μL. Furthermore, the electrochemical system exhibited more complete single-nucleotide discrimination capability, in accordance with the high selectivity of the Cas9-based sensing mechanism. By integrating amplification, detection, and control within a compact, smartphone-powered architecture, the system becomes a decentralized and field-deployable molecular diagnostic device. The platform focuses primarily on nucleic acid amplification and detection, while upstream sample preparation steps such as sample collection and processing (i.e., lysis and nucleic acid extraction) are performed off-chip. Future efforts will integrate these sample preparation modules, potentially through point-of-collection lysis and microfluidic processing strategies, to enable a fully enclosed end-to-end sample-to-answer diagnostic workflow. This study is an important step toward that goal and demonstrates a versatile and low-cost framework for point-of-care platforms while providing a practical foundation for future CRISPR-integrated biosensing technologies in pathogen surveillance, sample detection, and diagnostics.

Experimental

Materials and reagents

All reagents used in this work were of analytical grade. Sulfuric acid, potassium chloride, potassium ferrocyanide, potassium ferricyanide, absolute ethanol, poly(-diallyldimethylammonium chloride) solution (PDDA), cysteamine, glutaraldehyde, hexaammineruthenium(III) chloride (RuHex), Anti-CRISPR/CAS9 -FITC antibody, Mouse monoclonal, clone 7A9-3A3, purified from hybridoma cell culture were purchased from Sigma Aldrich (St. Louis, MO, United States); Monolayer graphene oxide water dispersant was purchased from MSE Supplies (Tucson, AZ, United States); Phusion U Multiplex PCR Master Mix, Tris–EDTA buffer and nuclease-free water were purchased from ThermoFisher Scientific (Waltham, MA, United States); All Primers, ultramers, and sgRNAs were purchased from Integrated DNA Technologies (Coralville, Iowa, United States); SpCas9 nuclease was purchased from Aldevron (Fargo, ND, United States); The sgRNA was purchased from Synthego (Redwood City, CA, United States); NEBuffer™ r3.1, WarmStart Multi-Purpose LAMP/RT-LAMP 2X Master Mix were purchased from New England Biolabs (Ipswich, MA, United States); The silver/silver chloride paste was purchased from Creative Materials, Inc. (Ayer, MA, United States).

Device fabrication

On-chip LIG heater fabrication

The on-chip heating module for the LAMP reaction was fabricated using laser writing on a polyimide (PI) substrate. A polyimide film was first adhered to the back side of a 200 μm thick PMMA sheet and patterned by carbon dioxide laser engraving to form the LIG heater. Laser irradiation locally carbonized the PI surface, generating a conductive graphene-like network that functions as a Joule heating element[56]. The complete on-chip LAMP structure consists of a three-layer laminated assembly. The top and bottom layers were fabricated from 200 μm thick PMMA sheets, while the 100 μm thick middle spacer layer was fabricated with PI-based double-sided adhesive tape to define the microfluidic chamber geometry. All layers were cut using precision laser machining to form alignment holes, inlet/outlet ports, and chamber outlines. The layers were then aligned and bonded under moderate pressure to ensure leak-free sealing and efficient thermal contact between the LIG heater and the LAMP reaction chamber. Electrical connections were established using copper tape and conductive silver paste at both ends of the LIG. Prior to device integration, the heater was characterized for temperature responsiveness and stability.

Microfluidic surface modification

As part of the integrated microfluidic system, the inner channel surfaces underwent a self-assembled graphene oxide hydrophilic treatment to enable liquid transport and confinement within the chambers[57,58]. Specifically, the microchannel surfaces were first covered with adhesive tape, and laser cutting was used to expose only the regions requiring modification. The exposed areas were alternately immersed in a PDDA solution with graphene oxide dispersion for 10 min each, with deionized water rinsing between steps. This cycle was repeated twice to form a uniform self-assembled graphene oxide coating. The treated surfaces exhibited significantly improved wettability, providing smooth liquid flow and enhanced stability of on-chip reactions.

Fabrication of electrochemical sensing electrodes

The electrochemical DNA sensor was constructed based on a standard three-electrode configuration, consisting of a gold working electrode, a counter electrode, and an Ag/AgCl reference electrode. The gold electrode pattern was defined on a glass substrate through photolithography to obtain a uniform and reproducible geometry. The reference electrode was prepared by applying Ag/AgCl paste directly onto the substrate surface and allowing it to dry naturally. Prior to modification, the gold electrode was cleaned by CV with 0.1 M H_2SO_4 until a stable voltammogram was obtained, ensuring a contaminant-free and reproducible surface.

Surface functionalization was achieved using a bifunctional molecular linker composed of cysteamine and glutaraldehyde[59]. The electrode was first immersed in a 10 mM cysteamine solution in absolute ethanol and incubated for 3 h in the dark to introduce amino groups on the gold surface. After rinsing with ethanol and deionized water, the electrode was treated with a 2.5% (w/w) glutaraldehyde aqueous solution for 30 min to introduce surface aldehyde groups for subsequent protein immobilization.

Cas9 and sgRNA were sequentially assembled on the functionalized surface to form the Cas9–sgRNA recognition layer. Specifically, 10 μL of Cas9 solution (10 μg μL^{-1}) was drop-cast onto the glutaraldehyde-activated electrode and incubated overnight at 4 °C to ensure efficient covalent attachment. After gentle rinsing with nuclease-free water to remove unbound protein, 10 μL (1 μg μL^{-1}) of sgRNA solution was added to the electrode surface and incubated for 1 h at room temperature to allow hybridization and formation of the Cas9–sgRNA complex. The modified electrodes were then rinsed again with nuclease-free water and stored in pH 7.4 phosphate-buffered saline (PBS) at 4 °C until used.

Characterization and measurement

Characterization of LIG heater and on-chip LAMP

The surface morphology of the LIG was examined using a field emission gun scanning electron microscope

(FEGSEM, Hitachi SU8230). Raman spectroscopy was conducted using a confocal Raman microscope to analyze the carbon structure. The heating performance of the LIG element was characterized by attaching a thermocouple between the LIG surface and the amplification chamber in the microfluidic chip. Temperature control was managed using a PID feedback system integrated into the Arduino microcontroller. Temperature stability and power consumption were recorded under various applied voltages to establish the heating–temperature relationship. The response time and steady-state behavior were monitored to evaluate the efficiency of on-chip temperature regulation for isothermal amplification.

Functionality of the integrated heating system was further verified through LAMP tests. LAMP primer sets were designed across the Spike gene of SARS-CoV-2, and their biotinylation strategy and performance were optimized as shown in Supplementary Fig. S1. LAMP reactions were performed under different temperature settings to determine optimal amplification conditions. Negative controls were prepared in parallel using reaction mixtures without target DNA to assess amplification specificity. After completion, the amplified products were collected and analyzed by agarose gel electrophoresis to verify successful DNA amplification and to confirm reaction selectivity.

LFA testing protocol

Synthetic DNA or RNA templates were used for the development of amplification and detection conditions. All DNA and RNA sequences, including templates, primers, guide RNAs, and blocking oligonucleotides, are detailed in the Supplementary Materials. All test nucleic acids were submitted to the University of Minnesota Genomics Center for quantification using PicoGreen.

For DNA amplification, the starting material was a synthetic, single-stranded molecule. PCR reactions were performed with initial denaturation at 98 °C for 30 s, followed by 35 cycles of denaturation at 98 °C for 10 s, annealing at 60 °C for 20 s, and extension at 72 °C for 5 s, with a final extension at 72 °C for 2 min. PCR products were confirmed by agarose gel electrophoresis and purified using a silica column-based PCR clean-up method, followed by elution in nuclease-free water. RNA transcripts were generated from DNA templates using PCR to add a T7 RNA polymerase sequence. These purified DNA templates were subjected to in vitro transcription to generate RNA, with the addition of an RNase inhibitor to prevent degradation. Products were resolved on an agarose gel, excised and purified using the Monarch® DNA Gel Extraction Kit (NEB; Ipswich, MA).

RNA at defined concentrations was subsequently used as input for RT-LAMP reactions using a WarmStart Multi-Purpose LAMP/RT-LAMP 2X Master Mix (with UDG) from NEB (Ipswich, MA). In a total reaction volume of 20 µL, inner primers (FIP and biotinylated BIP) were used at a final concentration of 1.6 µM, outer primers (F3 and B3) at 0.2 µM, and loop primers (LF or LB) at 0.4 µM. All primer sequences are provided in the Supplementary Materials.

For post-amplification copy number analysis, synthetic DNA templates were amplified by PCR using the 2X Phusion U Multiplex PCR master mix (ThermoFisher). Cycling conditions consisted of an initial denaturation at 98 °C for 30 s, followed by 40 cycles of denaturation at 98 °C for 10 s, annealing at 60 °C for 30 s, and extension at 72 °C for 10 s, with a final extension at 72 °C for 5 min. Amplified products were resolved by agarose gel electrophoresis, excised, purified by gel extraction, and quantified using a fluorescence-based double-stranded DNA assay.

Specificity analyses were conducted using synthetic single-nucleotide polymorphism templates amplified under identical PCR conditions. Amplified products from specificity and copy number assays were used directly for downstream detection.

For LFA detection, amplified DNA products were incubated with 10 µg of Cas9 protein and 1 µg of sequence-specific or non-homologous control single-guide RNA in the presence of 3 µg of FITC-labeled Cas9 antibody (Sigma Aldrich, St. Louis, MO). 25 µM double-stranded blocking oligonucleotide was included to suppress nonspecific Cas9–DNA interactions. Reactions were carried out in the NEB3.1 reaction buffer and adjusted to a final volume of up to 100 µL using a lateral flow running buffer. Detection was performed using commercial lateral flow assay strips (TwistDx Milenia HybriDetect1 lateral flow assay kit, Maidenhead, UK).

For LFAs in the presence of non-homologous or competitor DNA, we amplified DNA from HEK293T genomic DNA (see primer sequences in Supplementary information).

The biotinylated product (CXCR4) was incubated with SARS-CoV-2 sgRNA and evaluated by LFA following 1 h incubation with Cas9:FITC. The C7 amplicon was used in a 50:50 mixture (10 µl each amplicon) with SARS-CoV-2 target DNA and incubation with Cas9:SARS-CoV-2 sgRNA:FITC or a non-homologous control sgRNA. Similarly, following 60 min of incubation with Cas9, the products (20 µl total) were applied to LFA strips.

For wastewater detection using LFA, influent was obtained by overnight courier, and total nucleic acid was isolated using the Wizard® Enviro Total Nucleic Acid Kit (Promega, Madison, WI). For qRT-PCR, 5 µL of sample was used for analysis with the TaqPath COVID-19 Combo Kit (Thermo Fisher, Waltham, MA) that is a multiplex PCR assay with primers:probes for the SARS-CoV-2 N, Orf1a, and S genes. PCR was performed on the QuantStudio 5 Real-Time PCR instrument (Thermo Fisher, Waltham, MA). For LFA analysis, the eluate (1:5

dilution) was amplified using LAMP PCR with biotinylated primer followed by addition of Cas9:FITC.

Electrochemical measurements

Electrochemical tests were performed to evaluate both the interfacial characteristics and the sensing performance of the Cas9-based electrochemical sensor. The electrode modification process was characterized by CV and EIS. CV measurements were carried out in 5 mM $K_3[Fe(CN)_6]/K_4[Fe(CN)_6]$ containing 0.1 M KCl, within a range of −0.2 to +0.6 V at a scan rate of 100 mV·s^{-1}. EIS measurements were conducted over a frequency range of 10^{-1}–10^5 Hz with an amplitude of 10 mV.

After modification, the electrodes were incubated in the target DNA solution to allow specific binding between Cas9–sgRNA complexes and the target DNA. Subsequently, the electrodes were exposed to a RuHex solution for electrostatic interaction with the DNA phosphate backbone[60]. DNA incubation time, RuHex concentration, and incubation duration were systematically investigated in later experiments. After each step, electrodes were rinsed with nuclease-free water to remove unbound species.

DPV was employed to detect the redox signal of RuHex bound to the DNA layer. All measurements were performed in 50 mM Tris–EDTA buffer with the following parameters: start potential +0.3 V, stop potential −0.5 V, step potential 5 mV, modulation amplitude 25 mV, modulation time 0.01 s, interval time 0.1 s, and an effective scan rate of approximately 0.05 V·s^{-1}. All electrochemical experiments were conducted in a standard three-electrode configuration, and each test was repeated at least three times.

Acknowledgements

Portions of this work were conducted in the Minnesota Nano Center, which is supported by the National Science Foundation through the National Nano Coordinated Infrastructure Network (NNCI) under Award Number ECCS-1542202. Parts of this work were conducted in the Characterization Facility at the University of Minnesota, which receives partial support from the NSF through the MRSEC (Award Number DMR-2011401) and the NNCI (Award Number ECCS-2025124) programs. MJO is supported by the Minnesota Department of Health, the CDC Pathogen Genomics Centers of Excellence Network, and the NIH (2R01AR063070-11).

Author contributions

Peng Zhou and Amber N. McElroy: Methodology, Investigation, Data curation, Data analysis, Writing—original draft. Yingming Xu and Andrew Decker: Device fabrication and Electrical unit design. Timothy W. Schacker and Terrence W. Simon: Technical guidance, Review and Editing. Tianhong Cui and Mark J. Osborn (equal contributors): Supervision, Conceptualization, Project administration, Review, and editing.

Data availability

The data that support the findings of this study are available from the corresponding author upon reasonable request.

Conflict of interest

The authors declare no competing interests.

Supplementary information The online version contains supplementary material available at https://doi.org/10.1038/s41378-026-01340-y.

Received: 27 January 2026 Revised: 31 March 2026 Accepted: 13 April 2026
Published online: 03 June 2026

References

1. Horton, S. et al. Moving the dial on diagnostics: an update from the Lancet Commission on diagnostics. *Lancet* **405**, 2241–2254 (2025).
2. Shrestha, K. et al. Challenges in the development and implementation of point-of-care handheld qPCR devices. *Small* e06233. https://doi.org/10.1002/smll.202506233 (2025).
3. Larremore, D. B. et al. Test sensitivity is secondary to frequency and turnaround time for COVID-19 screening. *Sci. Adv.* **7**, eabd5393 (2021).
4. Chen, H., Liu, K., Li, Z. & Wang, P. Point of care testing for infectious diseases. *Clin. Chim. Acta* **493**, 138–147 (2019).
5. Herrmann, L. et al. Comparison of the diagnostic accuracy of the Pluslife Mini Dock RHAM technology with Abbott ID Now and Cepheid GenXpert: a retrospective evaluation study. *Sci. Rep.* **14**, 13978 (2024).
6. Karon, B. S. At-home molecular diagnostics: just around the corner or years away? *J. Appl. Lab. Med.* **9**, 168–171 (2024).
7. Martinez, A. W., Phillips, S. T., Whitesides, G. M. & Carrilho, E. Diagnostics for the developing world: microfluidic paper-based analytical devices. *Anal. Chem.* **82**, 3–10 (2010).
8. Rohrman, B. A. & Richards-Kortum, R. R. A paper and plastic device for performing recombinase polymerase amplification of HIV DNA. *Lab a Chip* **12**, 3082–3088 (2012).
9. Sun, A. et al. An integrated microfluidic platform for nucleic acid testing. *Microsyst. Nanoeng.* **10**, 66 (2024).
10. Zhang, Y. et al. A point-of-care microfluidic biosensing system for rapid and ultrasensitive nucleic acid detection from clinical samples. *Lab Chip* **23**, 3862–3873 (2023).
11. Bai, Y. et al. Signal amplification strategy of DNA self-assembled biosensor and typical applications in pathogenic microorganism detection. *Talanta* **272**, 125759 (2024).
12. Das, D., Lin, C. W. & Chuang, H. S. LAMP-based point-of-care biosensors for rapid pathogen detection. *Biosensors* **12**, 1068 (2022).
13. Zhang, H. et al. LAMP-on-a-chip: revising microfluidic platforms for loop-mediated DNA amplification. *TrAC Trends Anal. Chem.* **113**, 44–53 (2019).
14. Ye, R., James, D. K. & Tour, J. M. Laser-induced graphene: from discovery to translation. *Adv. Mater.* **31**, 1803621 (2019).
15. Bobinger, M. R. et al. Flexible and robust laser-induced graphene heaters photothermally scribed on bare polyimide substrates. *Carbon* **144**, 116–126 (2019).
16. Fan, X. et al. Graphene MEMS and NEMS. *Microsyst. Nanoeng.* **10**, 154 (2024).
17. Fang, M. et al. Novel nucleic acid detection based on the guide-independent nuclease activity of TbAgo. *Biosens. Bioelectron.* 118370. https://doi.org/10.1016/j.bios.2026.118370 (2026).
18. Dey, A. et al. Development of a rapid and ultra-sensitive RNA: DNA hybrid immunocapture based biosensor for visual detection of SARS-CoV-2 RNA. *PNAS Nexus* **2**, pgad031 (2023).
19. Xu, W. & Zhao, L. An enzyme-linked immunosorbent assay for the detection of mitochondrial DNA–protein cross-links from mammalian cells. *DNA* **2**, 264–278 (2022).
20. Jiang, L. et al. Current research status of tumor cell biomarker detection. *Microsyst. Nanoeng.* **9**, 123 (2023).
21. Li, Y., Li, S., Wang, J. & Liu, G. CRISPR/Cas systems towards next-generation biosensing. *Trends Biotechnol.* **37**, 730–743 (2019).
22. Broughton, J. P. et al. CRISPR–Cas12-based detection of SARS-CoV-2. *Nat. Biotechnol.* **38**, 870–874 (2020).
23. Li, L. et al. HOLMESv2: a CRISPR-Cas12b-assisted platform for nucleic acid detection and DNA methylation quantitation. *ACS Synth. Biol.* **8**, 2228–2237 (2019).
24. Aquino-Jarquin, G. CRISPR-Cas14 is now part of the artillery for gene editing and molecular diagnostic. *Nanomed.: Nanotechnol., Biol. Med.* **18**, 428–431 (2019).
25. Gootenberg, J. S. et al. Nucleic acid detection with CRISPR-Cas13a/C2c2. *Science* **356**, 438–442 (2017).

26. Kellner, M. J., Koob, J. G., Gootenberg, J. S., Abudayyeh, O. O. & Zhang, F. SHERLOCK: nucleic acid detection with CRISPR nucleases. *Nat. Protoc.* **14**, 2986–3012 (2019).
27. Xu, W., Jin, T., Dai, Y. & Liu, C. C. Surpassing the detection limit and accuracy of the electrochemical DNA sensor through the application of CRISPR Cas systems. *Biosens. Bioelectron.* **155**, 112100 (2020).
28. Sandler, S. E. et al. Sensing the DNA-mismatch tolerance of catalytically inactive Cas9 via barcoded DNA nanostructures in solid-state nanopores. *Nat. Biomed. Eng.* **8**, 325–334 (2024).
29. Wang, X. et al. Clustered regularly interspaced short palindromic repeats/Cas9-mediated lateral flow nucleic acid assay. *ACS Nano* **14**, 2497–2508 (2020).
30. Osborn, M. J. et al. CRISPR/Cas9-based lateral flow and fluorescence diagnostics. *Bioengineering* **8**, 23 (2021).
31. Liu, M. et al. A portable self-powered turbine spirometer for rehabilitation monitoring on COVID-19. *Adv. Mater. Technol.* **8**, 2300328 (2023).
32. Xue, Z., Gai, Y., Wu, Y., Liu, Z. & Li, Z. Wearable mechanical and electrochemical sensors for real-time health monitoring. *Commun. Mater.* **5**, 211 (2024).
33. Rasheed, S. et al. Advances and challenges in portable optical biosensors for onsite detection and point-of-care diagnostics. *TrAC Trends Anal. Chem.* **173**, 117640 (2024).
34. Srisomwat, C. et al. Amplification-free DNA sensor for the one-step detection of the hepatitis B virus using an automated paper-based lateral flow electrochemical device. *Anal. Chem.* **93**, 2879–2887 (2020).
35. Jauset-Rubio, M. et al. Ultrasensitive, rapid and inexpensive detection of DNA using paper based lateral flow assay. *Sci. Rep.* **6**, 37732 (2016).
36. Takalkar, S., Baryeh, K. & Liu, G. Fluorescent carbon nanoparticle-based lateral flow biosensor for ultrasensitive detection of DNA. *Biosens. Bioelectron.* **98**, 147–154 (2017).
37. Drummond, T. G., Hill, M. G. & Barton, J. K. Electrochemical DNA sensors. *Nat. Biotechnol.* **21**, 1192–1199 (2003).
38. Jampasa, S. et al. Multiple signaling probe-based ultrasensitive electrochemical DNA sensor integrated with NFC-enabled smartphone to diagnose leptospirosis. *Sens. Actuators B Chem.* **406**, 135411 (2024).
39. Zhang, L. et al. Recent progresses in electrochemical DNA biosensors for MicroRNA detection. *Phenomics* **2**, 18–32 (2022).
40. Cong, L. et al. Multiplex genome engineering using CRISPR/Cas systems. *Science* **339**, 819–823 (2013).
41. Lin, J. et al. Laser-induced porous graphene films from commercial polymers. *Nat. Commun.* **5**, 5714 (2014).
42. Li, D. et al. Design and thermal analysis of flexible microheaters. *Micromachines* **13**, 1037 (2022).
43. Hardinge, P., Kiddle, G., Tisi, L. & Murray, J. A. Optimised LAMP allows single copy detection of 35Sp and NOSt in transgenic maize using Bioluminescent Assay in Real Time (BART). *Sci. Rep.* **8**, 17590 (2018).
44. Ahn, S. J., Costa, J. & Rettig Emanuel, J. PicoGreen quantitation of DNA: effective evaluation of samples pre- or post-PCR. *Nucleic Acids Res.* **24**, 2623–2625 (1996).
45. Melvin, R. G. et al. A novel wastewater-based epidemiology indexing method predicts SARS-CoV-2 disease prevalence across treatment facilities in metropolitan and regional populations. *Sci. Rep.* **11**, 21368 (2021).
46. Granato, P. A., Kimball, S. R., Alkins, B. R., Cross, D. C. & Unz, M. M. Comparative evaluation of the Thermo fisher TaqPath™ COVID-19 combo kit with the Cepheid Xpert® Xpress SARS-CoV-2 assay for detecting SARS-CoV-2 in nasopharyngeal specimens. *BMC Infect. Dis.* **21**, 623 (2021).
47. McMillen, T., Jani, K., Robilotti, E. V., Kamboj, M. & Babady, N. E. The spike gene target failure (SGTF) genomic signature is highly accurate for the identification of Alpha and Omicron SARS-CoV-2 variants. *Sci. Rep.* **12**, 18968 (2022).
48. Cirrincione, M. et al. Assessment of reader technologies for over-the-counter diagnostic testing. *IEEE Open J. Eng. Med. Biol.* **5**, 210–215 (2024).
49. Zhang, K. et al. Direct visualization of single-nucleotide variation in mtDNA using a CRISPR/Cas9-mediated proximity ligation assay. *J. Am. Chem. Soc.* **140**, 11293–11301 (2018).
50. Paquet, D. et al. Efficient introduction of specific homozygous and heterozygous mutations using CRISPR/Cas9. *Nature* **533**, 125–129 (2016).
51. Arduini, A., Laprise, F. & Liang, C. SARS-CoV-2 ORF8: a rapidly evolving immune and viral modulator in COVID-19. *Viruses* **15**, 871 (2023).
52. Zhang, Y. et al. The ORF8 protein of SARS-CoV-2 mediates immune evasion through down-regulating MHC-I. *Proc. Natl. Acad. Sci.* **118**, e2024202118 (2021).
53. Jung, W. J., Park, S. J., Cha, S. & Kim, K. Factors affecting the cleavage efficiency of the CRISPR-Cas9 system. *Anim. Cells Syst.* **28**, 75–83 (2024).
54. Longo, M. C., Berninger, M. S. & Hartley, J. L. Use of uracil DNA glycosylase to control carry-over contamination in polymerase chain reactions. *Gene* **93**, 125–128 (1990).
55. Dawoud, A., Mia, R., Motchaalangaram, J. A., Miao, W. & Wallace, K. Toward Remote Detection of Chemical Warfare Simulants Using a Miniature Potentiostat. *Micro* **4**, 49–60 (2024).
56. Xu, Y., Zhou, P. & Cui, T. Laser-induced graphene sensors with electropolymerized molecularly imprinted polymer for ultra-low perfluorooctanoic acid detection. *Sens. Actuators B Chem.* 138635. https://doi.org/10.1016/j.snb.2025.138635 (2025).
57. Zhou, P. & Cui, T. Enhanced photocatalytic efficiency by layer-by-layer self-assembly of graphene and titanium dioxide on shrink thermoplastic film. *Microsyst. Technol.* **26**, 3793–3798 (2020).
58. Hu, X., Yu, Y., Hou, W., Zhou, J. & Song, L. Effects of particle size and pH value on the hydrophilicity of graphene oxide. *Appl. Surf. Sci.* **273**, 118–121 (2013).
59. Ionescu, R. E. Use of cysteamine and glutaraldehyde chemicals for robust functionalization of substrates with protein biomarkers—an overview on the construction of biosensors with different transductions. *Biosensors* **12**, 581 (2022).
60. Wu, D., Yin, B. C. & Ye, B. C. A label-free electrochemical DNA sensor based on exonuclease III-aided target recycling strategy for sequence-specific detection of femtomolar DNA. *Biosens. Bioelectron.* **28**, 232–238 (2011).